Available online at www.sciencedirect.com
SCIENCE DIRECT®

Journal of the European Ceramic Society 24 (2004) 3111–3118

www.elsevier.com/locate/jeurceramsoc

Effect of ZrO_2 additions on sintering of SnO_2-based ceramics

A. Maître*, D. Beyssen, R. Podor

Laboratoire de Chimie du Solide Minéral, UMR CNRS 7555, Université Henri Poincaré, Bd des Aiguillettes, BP 239, F-54506 Vandoeuvre-Les-Nancy cedex, France

Received 12 June 2003; received in revised form 24 October 2003; accepted 8 November 2003

Abstract

The effect of zirconia additions on sintering of CoO doped tin dioxide has been investigated in the temperature range 1100–1250 °C. A first study showed that the substitution of tin by zirconium reduces significantly the volatilisation rate of SnO_2 for temperatures greater than 1400 °C. It appeared that the zirconium content increase inhibits the densification kinetics of SnO_2-based ceramics. Indeed, the relative density did not exceed 93% for a Zr content lower than 6 mol% in the $Sn_{(1-x)}Zr_xO_2$ solid solution. This negative effect can be imputed to the elastic distortions caused by the introduction of Zr in the tin dioxide lattice. So, the diffusion rate of point defects such as oxygen or cobalt ions is lowered.

Keywords: Diffusion; Point defects; Sintering; SnO_2; ZrO_2

1. Introduction

Tin oxide polycristalline ceramics are n-type semiconductors that have been widely used in humidity and carbon monoxide sensors,[1–4] in thin films, solar cells and protective coatings,[5–8] as electrodes for electric glass melting furnaces and for electrochromic windows.[9,10] It is known that pure SnO_2 is unfortunately difficult to densify by natural sintering because of the predominance of non-densifying mechanisms for mass transport, such as surface diffusion and evaporation-condensation[11] which only promote pure coarsening and grain growth.

The use of ultrafine SnO_2 powders compacted under very high pressure[12] and/or the employing of hot isostatic pressing technique offer solutions for preparing highly-densified SnO_2 ceramics. However, it also appears that only additions of small amounts of sintering additives favour densification: for example, a liquid phase sintering mechanism is induced when the additive used is CuO[13] whereas MnO_2, CoO and Li_2O are additives known to form solid solution with SnO_2.[14]

In the case of specific applications of SnO_2-based materials such as heating electrodes where these materials can be in direct contact with metallic pieces at temperature higher than 700 °C, the use of additives such as ZrO_2 seems to be necessary in order to reduce the tin activity in SnO_2 by substitution of Sn. On this subject, a recent work[15] demonstrated the existence of a $(Sn_{1-x}Zr_x)O_2$ solid solution (with $x \leqslant 0.26$). Moreover, it can be supposed that at temperatures higher than 1300 °C ZrO_2 additions could retard the decomposition kinetic of tin dioxide according to the equation:

$$SnO_{2(s)} \rightarrow SnO_{(s)} + \frac{1}{2}O_{2(g)} \quad (1)$$

The aim of the present work is to examine the sintering of tin dioxide in terms of zirconia content and with a constant cobalt monoxide content.

2. Experimental procedure

2.1. Starting materials

Zirconium dioxide, tin dioxide and cobalt monoxide were supplied by GoodFellow™, Cerac™ and Aldrich™ respectively. Their main physical-chemistry characteristics are reported in Table 1. The average

* Corresponding author. Tel.: +33-3-83-68-46-56; fax: +33-3-83-68-46-11.
E-mail address: alexandre.maitre@lcsm.uhp-nancy.fr (A. Maitre).

0955-2219/$ - see front matter © 2003 Elsevier Ltd. All rights reserved.
doi:10.1016/j.jeurceramsoc.2003.11.009

grain sizes of the ceramic powders were calculated from the specific surface area determined by the BET method with a Sorptomatic 1990 Thermoquest apparatus:

$$\phi_m = \frac{6}{\rho\, S_{BET}} \quad (2)$$

where ρ is the powder density (g/cm^3), S_{BET} the specific area (m^2/g). The SEM observations of the starting powders (Fig. 1) show that the elementary particles present a quasi-spherical shape with an average grain size between 0.2 and 1 μm.

2.2. Apparatus and experimental conditions

The three powders (ZrO_2, SnO_2, CoO) were mixed in a first step in an agate mortar and then dispersed in pure ethanol with a Turbula apparatus. The powders were then dried at 120 °C for 12 h.

Discs of 13 mm diameter were uniaxially pressed under a pressure of 222 MPa. Densities were obtained by the Archimedes method (precision: 0.5% of relative density). Theoretical density of the mixture was calculated using the mixing law. The theoretical densities of ZrO_2, SnO_2 and

Table 1
Main characteristics of the starting powders

Powder (supplier)	Density (g.cm^{-3})	Specific area (m^2.g^{-1})	Granulometry (μm)	
			From Eq. (2)	By image analysis
SnO_2(Cerac^{TM})	6.95	16.8	0.5	0.2
ZrO_2(GoodFellow^{TM})	5.89	6.1	0.2	0.2
CoO(Aldrich^{TM})	6.45	4.4	0.2	1.1

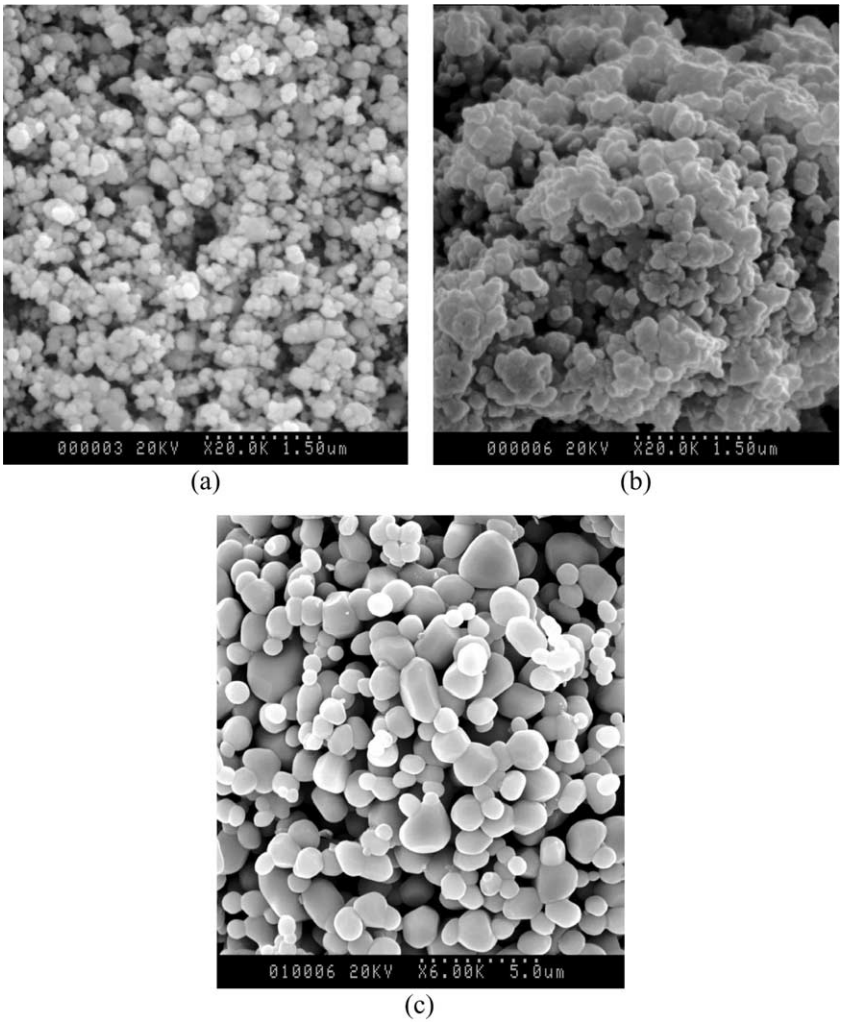

Fig. 1. SEM observations of SnO_2 (Cerac^{TM}) (a), ZrO_2 (Goodfellow^{TM}) (b) and CoO (Aldrich^{TM}) (c) powders.

CoO are 5.82 g/cm^3, 6.99 g/cm^3, 6.45 g/cm^3 respectively. Densities of cold-pressed samples were equal to about 60% of the theoretical. In order to determine the open porosity ratio, the geometric densities were also measured.

Thermogravimetric and differential thermal analyses were performed using a Setaram TGA92 equipment. Dilatometric measurements were performed using a Setaram TMA92 dilatometer. The heating rate was kept at 10 °C/min. To obtain a network of points showing relative density as a function of time, the samples were sintered in a Nabertherm furnace (LHT 04/17 model). The furnace was brought to the required temperature one hour before the sample introduction. Sample introduction and removal from the hot zones takes about 1 min.

After sintering, the samples were polished to obtain a mirror-like surface (diamond spray 1 μm). Grain boundaries were revealed by thermal etching at 1300 °C for three minutes assuming that this further heat treatment did not modify the initial grain size. The microstructures were examined using scanning electron microscopy (Philips XL 30 or Hitachi S2500). The zirconium content in SnO_2-based ceramics and the chemical composition of phases precipitated at grain boundaries were determined by electron microprobe analysis (EPMA- CAMECA SX 100). The morphology and the composition of the secondary phase that precipitated at the grain boundary were obtained by a transmission electron microscope (Philips CM20) operating at 200 kV and equipped with an energy dispersive X-ray spectrometer (EDXS). The thin foils were prepared by cutting plates 100 μm thick, then thinned by an argon ion-beam thinning method (Gatan-Model 691 apparatus).

3. Results

3.1. Choice of the sintering parameters

The addition of 0.5 mol% of CoO to the initial SnO_2–ZrO_2 mixtures was systematically performed in order to keep the geometric shape of specimens after thermal treatment and so, to determine the relative density. Therefore, the use of cobalt monoxide as sintering additive is due to the fact that low contents of CoO permit obtaining a significant densification of SnO_2-based materials[16,17] between 1100 and 1400 °C, i.e. less than the vaporization temperature of tin dioxide. From the phase diagram available in the literature,[17] it appears that a study of SnO_2–ZrO_2 ceramic sintering in the solid solution domain ($Sn_{(1-x)}Zr_xO_2$ with $x < 10$ mol%) can be performed.

3.1.1. Study of vaporisation of SnO_2–ZrO_2 solid solutions

TG experiments have been done for SnO_2-0.5 mol% CoO specimens and for several additions of zirconia. The thermal cycle used is presented on Fig. 2. The weight losses measured are reported as a function of the temperature ($T = 1100$, 1300, 1350, 1400 and 1450 °C) and of the ZrO_2 content in Fig. 3 and 4 respectively.

Fig. 3 shows that there is no weight loss below 1300 °C and that the volatilisation rate remains low between 1300 and 1450 °C. These results are in good agreement with those obtained for pure SnO_2 by Lalande et al.[13]

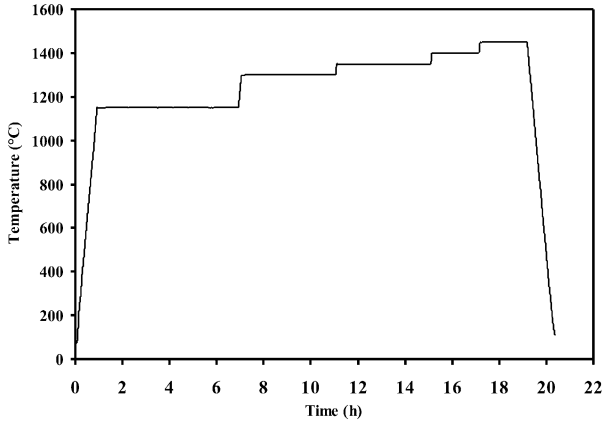

Fig. 2. Thermal cycling used for the determination of the weight loss for SnO_2-based materials.

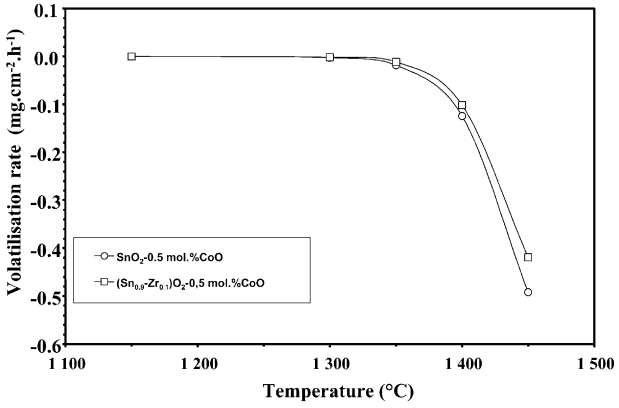

Fig. 3. Volatilisation rate as a function of the temperature for SnO_2–0.5mol%CoO and for a specimen containing 10 mol% of ZrO_2.

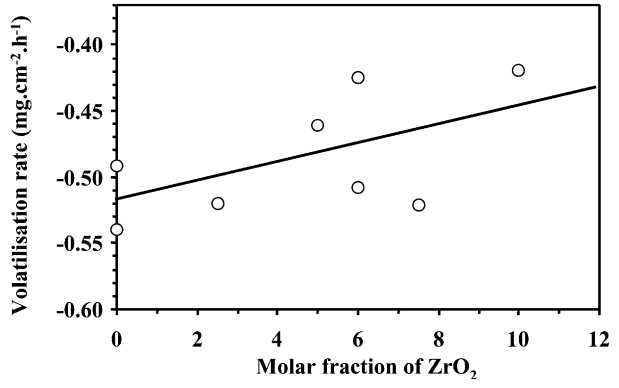

Fig. 4. Volatilisation rate as a function of the zirconium content in SnO_2-based material.

Comparison of the volatilisation rates obtained at 1450 °C for several $(Sn_{(1-x)}Zr_x)O_2$–0.5 mol%CoO materials suggests a limited decrease of the volatilisation rate with increasing zirconia content (Fig. 4).

Since the decomposition mechanism of $SnO_{2(s)}$ following Eq. (1) seems to be activated by temperature, it becomes possible to determine its apparent activation energy (E_A) from an Arrhenius representation (Fig. 5). The E_A values determined for all of the zirconium contents are similar. The average activation energy is equal to 815±40 kJ.mol^{-1}. This value is higher than those of the dissociation enthalpy of $SnO_{2(s)}$ measured using the Knudsen method by Hoenig et al.,[18] i.e. 567 kJ.mol^{-1}. This divergence can be imputed to the introduction of cobalt monoxide and zirconia in the present study. Indeed, by favouring the densification of SnO_2 ($\rho/\rho_0 \geqslant 99\%$) materials, the cobalt monoxide limits its reactivity at high temperature with regards to the reactivity of the hot pressed specimens ($\rho/\rho_0 \leqslant 97\%$) used by Hoenig et al.[18]

3.1.2. Dilatometry

Fig. 6 shows dimension changes ($\Delta L/L$) versus temperature for dilatometry experiments carried out using a heating rate of 5 °C/min from room temperature to 1400 °C, then a cooling rate of 10 °C/min. Moreover,

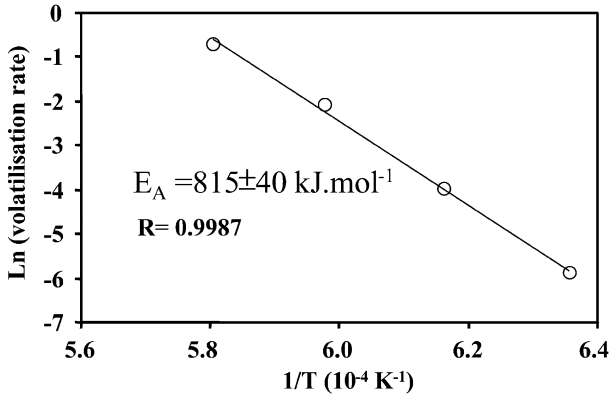

Fig. 5. Arrhenius representation of the volatilisation rate determined for the SnO_2–0.5 mol% material.

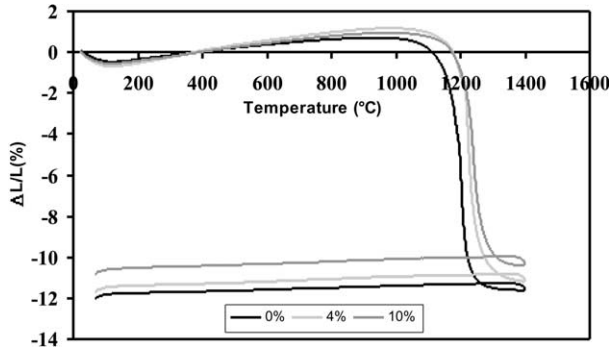

Fig. 6. Dilatometry results for $Sn_{1-x}Zr_xO_2$–0.5mol%CoO ceramics ($\Delta L/L$) as a function of temperature and of zirconium content.

Fig. 7 gives the shrinkage rate as a function of the ZrO_2 content of materials sintered at 1400 °C using the same heating and cooling rates as those used for the dilatometry experiments.

The temperature of the maximum of the shrinkage rate (T_M) determined from dilatometry experiments (see Fig. 6) separates the sintering into two temperature domains as indicated by Lange:[19]

- for $T < T_M$: the densifying mechanisms dominate the sintering of the SnO_2-based materials;
- for $T > T_M$: the non-densifying processes, such as the grain growth control the sintering.

In the present case, zirconia additions induce, on one hand, a rise of the (T_M) value and on the other, a limitation of the densification ratio (see Table 2). So, tin dioxide density without ZrO_2 addition culminates at 97.8% of theoretical value whereas the material with 10 mol% of ZrO_2 only reaches 83%.

Moreover, the addition of 10 mol% of zirconia to SnO_2 ceramic is accompanied by a rise of about 40 °C of the temperature of the maximum of the shrinkage rate.

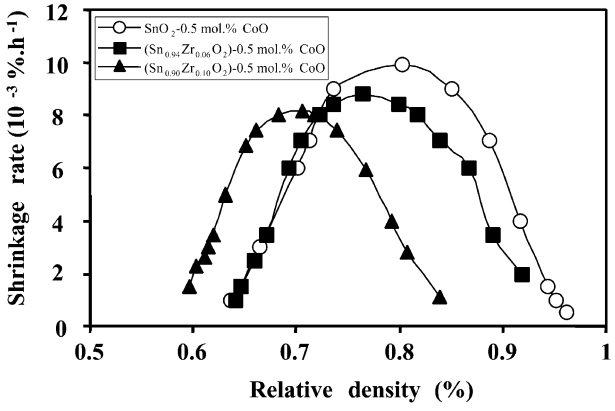

Fig. 7. Shrinking rate vs. relative density for $Sn_{1-x}Zr_xO_2$–0.5mol%-CoO materials.

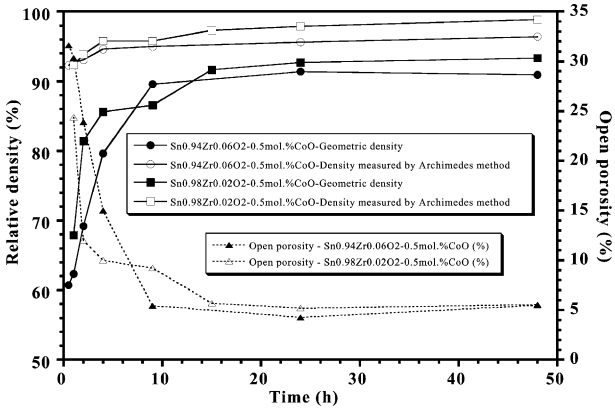

Fig. 8. Relative density determined by two methods vs. sintering time for $Sn_{0.98}Zr_{0.02}O_2$–0.5mol%CoO and $Sn_{0.96}Zr_{0.04}O_2$–0.5mol% CoO ceramics sintered at 1100 °C.

Comparison of the T_M value for SnO_2–0.5 mol% CoO ceramic obtained (≈1203 °C) with those determined by Cerri et al.[15] (≈1240 °C) shows a small discrepancy. This is certainly due to the difference of granulometry between the starting powders used. Indeed, several authors[16,17] indicate that the sintering of SnO_2–0.5mol% CoO is controlled by O^{2-} diffusion in the solid state. As it is well known, this diffusion process in the oxides strongly depends on the defect chemistry, i.e. on the nature and concentration of foreign atoms such as cobalt and also on the efficient contact number between CoO and SnO_2 grains.[20] Besides, this contact number increases with the average grain size decrease as demonstrated by the Cournil–Thomas formulae.[21]

From all of these results, it appears that the optimum temperature range for the sintering investigation is 1100–1250 °C. So, in a first step, the effect of the ZrO_2 addition on the densification kinetic was studied.

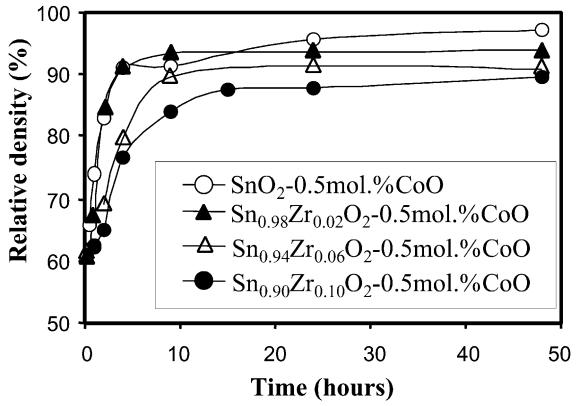

Fig. 9. Densification vs. sintering time at 1100 °C for different zirconium contents of $Sn_{1-x}Zr_xO_2$–0.5mol% CoO solid solution.

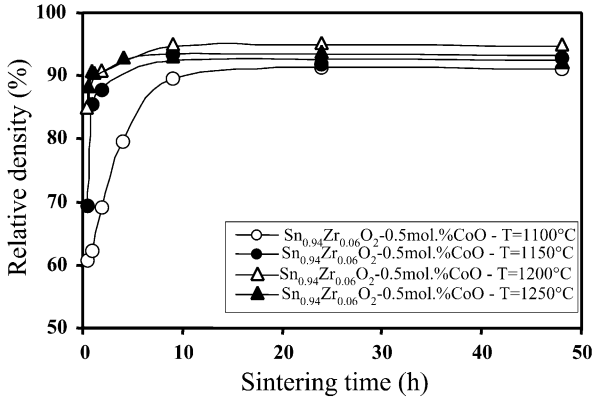

Fig. 10. Densification vs. sintering time for $Sn_{0.94}Zr_{0.06}O_2$-0.5mol%-CoO ceramic sintered between 1100 and 1250 °C.

3.2. Densification kinetics

The densification kinetics obtained for $(Sn_{(1-x)}Zr_x)O_2$–0.5 mol% CoO (with $x = 0.00$, 0.02, 0.04, 0.06, 0.08 and 0.10) are reported as a function of the temperature and zirconium content in Figs. 8, 9 and 10. The densities determined by the Archimedes method are compared

Table 2
Relative density and temperature of maximum shrinkage rate (T_M) after sintering of SnO_2–0.5mol% CoO pellets containing different concentration of ZrO_2

Sample	Temperature of the maximum shrinkage rate (T_M) (°C)	Relative density (%)
SnO_2-0.5 mol% CoO	1203	97.8
$(Sn_{0.98}Zr_{0.02})O_2$–0.5 mol% CoO	1213	97.7
$(Sn_{0.96}Zr_{0.04})O_2$–0.5 mol% CoO	1230	95.8
$(Sn_{0.94}Zr_{0.06})O_2$–0.5 mol% CoO	1235	94.5
$(Sn_{0.92}Zr_{0.08})O_2$–0.5 mol% CoO	1239	90.7
$(Sn_{0.90}Zr_{0.10})O_2$–0.5 mol% CoO	1243	88.2

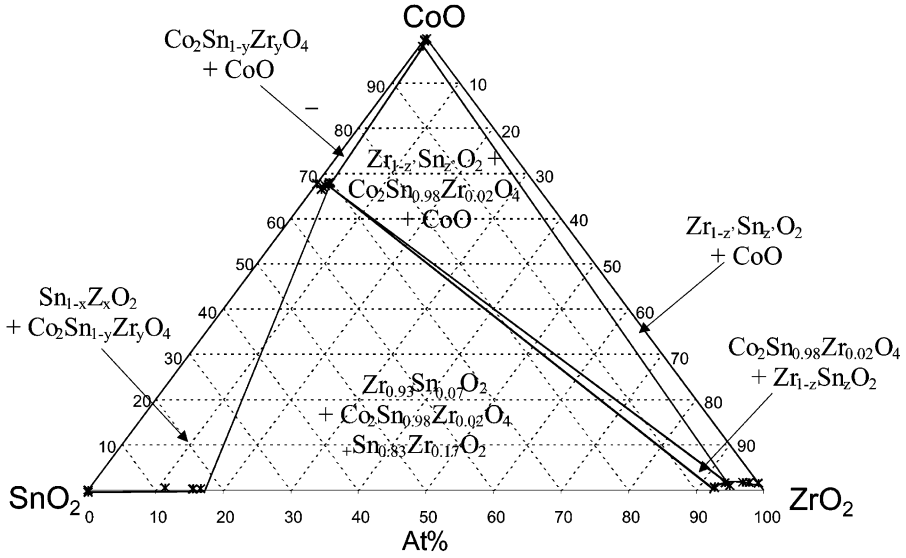

Fig. 11. Isotherm section at 1300 °C of the CoO–SnO_2–ZrO_2 pseudo-ternary phase diagram.

with the geometrical ones in order to obtain the evolution of the open porosity during the sintering process (see Fig. 8). It appears that the open porosity ratio dramatically drops for treatment times inferior to 10 h independently of the zirconium content. Conversely, the increase of the Zr content in SnO_2–0.5 mol% CoO induces a relative density decrease (see Fig. 9): after 48 h, the ZrO_2 free–SnO_2 ceramic reaches 97% of the theoretical density whereas the addition of 6 mol% of zirconia induces a limitation of 90%. Moreover, comparison of the densification kinetics obtained at different temperatures for $Sn_{0.94}Zr_{0.06}O_2$–0.5mol%CoO material (Fig. 10) demonstrates that the sintering mechanism is kinetically activated by temperature.

From all of these results, it appears that the substitution of tin element by zirconium in the solid solution plays a defavourable role on the kinetic of the densification mechanism: indeed, the relative density never overlaps 93% independently of the temperature level for $Sn_{0.94}Zr_{0.06}O_2$–0.5mol%CoO ceramic.

4. Discussion

In the literature, it is underlined[15,16] that the densification of CoO-doped SnO_2 is promoted by enhanced solid state diffusion from oxygen vacancy creation. Since the oxygen is the rate-controlling diffusion species, the sintering is improved by CoO doping, i.e. by an oxygen vacancy increase. To explain the negative effect of zirconia addition on the sintering of tin dioxide based materials, three possible explanations can be proposed.

In a first way, the densification rate decrease could be imputed to a cobalt solubility decrease in the SnO_2 lattice with zirconia content increase. On this subject, it appeared necessary to determine the isothermal section of the pseudo-ternary system CoO–SnO_2–ZrO_2 at the usual sintering temperature (i.e. 1300 °C) (Fig. 11). This was obtained from about 20 samples treated for 24 h at 1300 °C then air quenched. The observation of the phase diagram (Fig. 11) reveals a weak CoO solubility in tin dioxide (# 100 ppm by EPMA analysis) regardless

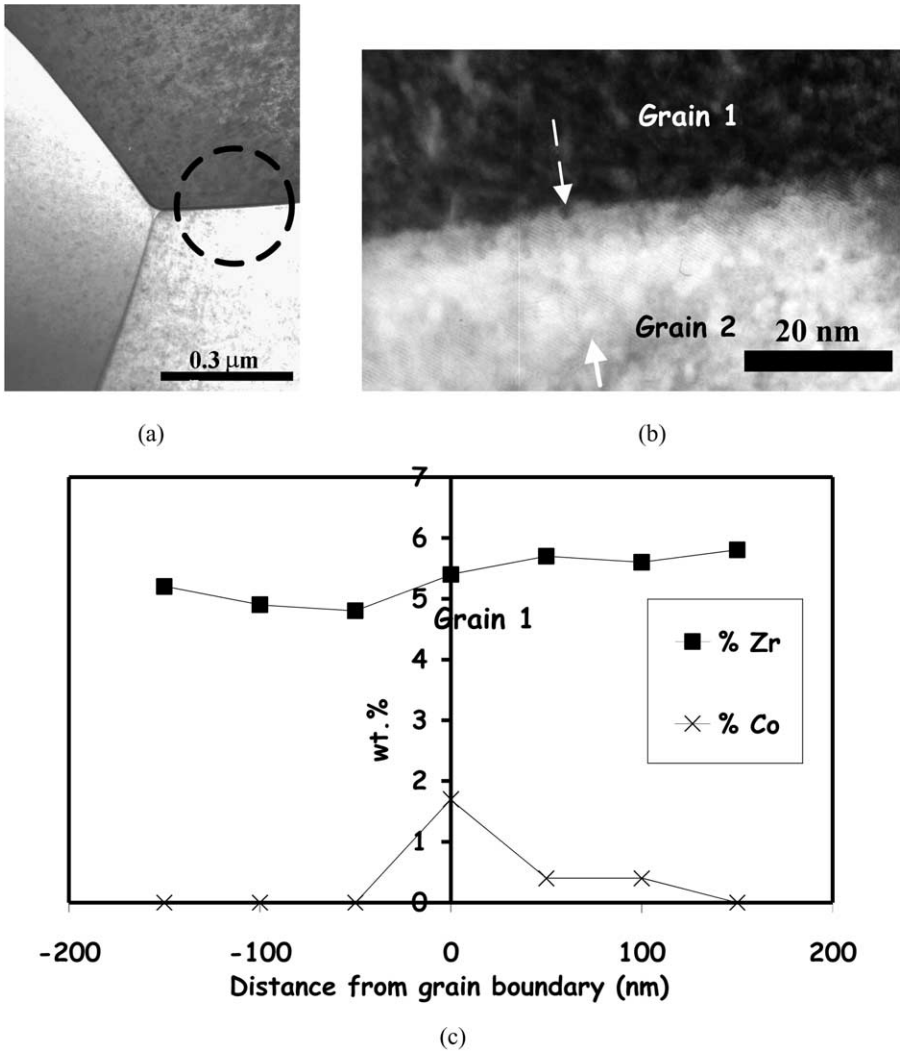

Fig. 12. TEM bright field micrographs at different magnitudes ([$1\bar{0}1$] axis zone) (a), (b) and EDXS analysis across the grain boundary (c) for the $Sn_{0.94}Zr_{0.06}O_2$–0.5mol% CoO ceramic after a sintering time of 24 h at 1200 °C.

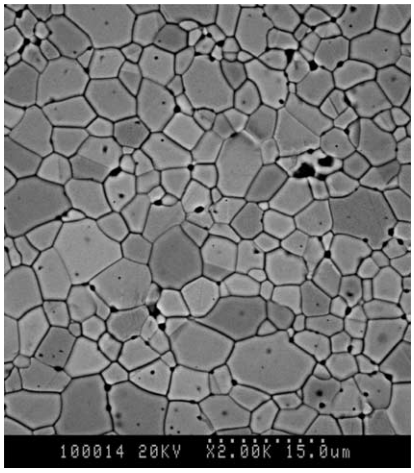

Fig. 13. SEM micrograph of the $Sn_{0.94}Zr_{0.06}O_2$–0.5mol% CoO ceramic after a sintering of 24 h at 1250 °C.

zirconium content in the $Sn_{(1-x)}Zr_xO_2$ solid solution. Moreover, the zirconium content rise in solid solution is accompanied by the same effect for the $Co_2Sn_{(1-y)}Zr_yO_4$ phase. Nevertheless, in this latter case, the final zirconium content remains inferior to 2 mol%. Consequently, for all the investigated compositions in the SnO_2–ZrO_2–CoO system and also corresponding to the compounds previously prepared, the samples are composed after heat treatment of both $Sn_{(1-x)}Zr_xO_2$ and $Co_2Sn_{(1-y)}Zr_yO_4$ solid solutions. So, it is not possible to explain the negative effect of zirconia additions by a free zirconia precipitation which could induce some residual stress during cooling by the martensitic transformation "monoclinic ↔ tetragonal" of ZrO_2.

In a second way, it can be suggested that the main physical characteristics of the $Co_2Sn_{(1-y)}Zr_yO_4$ phase would be modified by its zirconium content. In particular, it can be supposed that this phase melts during the sintering treatment. Nevertheless, from TEM and associated EDXS investigations (Fig. 12), only a thin and well crystallised secondary phase was detected at the grain boundary (probably $Co_2Sn_{(1-y)}Zr_yO_4$ solid solution from the phase diagram of Fig. 11). Consequently, with regards to the CoO–SnO_2–ZrO_2 phase diagram section determined in this study, it can be concluded that no new compound between cobalt oxide, tin dioxide and zirconium dioxide with a low melting temperature was formed.

Finally, the role played by zirconia additions on both electrostatic and elastic interactions between point defects must be more precisely taken into account. The introduction of CoO in the SnO_2 lattice (without Zr) is usually compensated by oxygen vacancies ($V_O^{\bullet\bullet}$) following:[15,22]

$$CoO \xrightarrow{SnO_2} Co''_{Sn} + V_O^{\bullet\bullet} + O_O \quad (3)$$

The small size mismatch between Co^{2+} (0.65 Å) and Sn^{4+} (0.69 Å)[23] does not induce elastic distortions. Consequently, Co''_{Sn} maintains a strong electrostatic attraction with $V_O^{\bullet\bullet}$ and this leads to the formation of an associated defect ($Co''_{Sn} + V_O^{\bullet\bullet}$) due to their coulomb attraction. With zirconia additions, the size mismatch due to Zr^{4+} (0.73 Å) substitution is higher[23] and implies a non negligible increase of the elastic deformations that could destroy the point defect association by increasing the overall strain. Some microstructural observations (Fig. 13) of the sintered material with preliminary additions of ZrO_2 show the presence of many defects and closed porosity within the bulk of the SnO_2 grains. For ZrO_2 free materials, a similar morphology has not been detected because $V_O^{\bullet\bullet}$ and Co''_{Sn} point defects probably diffuse more rapidly to the grain boundary forming the $Co_2Sn_{(1-y)}Zr_yO_4$ secondary phase.

5. Conclusion and outlook

The sintering of $Sn_{(1-x)}Zr_xO_2$.0.5mol%CoO was investigated in the temperature range (1100–1250 °C). It has been shown that zirconia additions limit the densification of the SnO_2-based materials. This effect can be imputed to the elastic distortions in the SnO_2 lattice due to a significant size mismatch between Zr^{4+} and Co^{2+} ions. Consequently, the diffusion rate of associate defects ($V_O^{\bullet\bullet} + Co''_{Sn}$) is reduced and this induces closed porosity within the bulk in SnO_2 grains.

A next study will involve the investigation of the secondary phase role upon the densification and the grain growth mechanisms. It will be interesting to evaluate its effect as a function of Zr content on the interfacial transport properties.

Acknowledgements

The authors are pleased to thank Lionel Aranda for technical help, specially during the TG and dilatometry experiments, A. Kohler for MEB studies and F. Diot for EPMA analyses.

References

1. Fagan, J. G. and Amarakoon, V. R., Reliability and reproducibility of ceramic sensors. Part III. Humidity sensors. *Am. Ceram. Soc. Bull.*, 1993, **72**, 119–124.
2. Tsai, P. P., Chen, J. C. and Tzeng, M. H., Tin oxide (SnOx) alcohol sensor from metal organic decomposed (MOD) thick film. *Sensors Actuators B*, 1995, **14**, 610–612.
3. Jaffrezic-Renault, N., Pijolat, C., Pauly, A., Brunet, J., Varenne, C., Bouvet, M. and Fabry, P., Materials for chemical sensors. *Actualité Chimique*, 2002, **3**, 157–171.
4. Lalauze, R., Pijolat, C., Tournier, G. and Breuil, B., Tin dioxide sensor a very complex device: physico-chemical and technological approach. *Electron Technology*, 2000, **33**, 31–39.
5. Li, X., Wanlass, M. W., Gessert, T. A., Emery, K. A. and Coutts,

T. J., High-efficiency indium tin oxide/indium phosphide solar cells. *Applied Physics Letters*, 1989, **54**, 2674–2676.
6. Coutts, T. J., Persall, N. M. and Tarricone, T., The influence of input power on the performance of rf sputtered ITO/indium phosphide solar cells. *J. Vacuum Sci. Technol. B*, 1984, **2**, 140.
7. Deimel, P. P., Heimofer, B. B. and Voges, E., *IEEE Photonic Technol. Lett*., 1990, **2**, 499.
8. Jackson, N. and Ford, J., Experience in the control and evaluation of coatings on glass containers. *Thin Solid Films*, 1981, **77**, 23–39.
9. Panteleev, V. G., Ramm, K. S. and Pron'kina, T. I., Effect of the structure of tin oxide ceramics on their glass resistance. *Glass Ceramics*, 1990, **46**, 199.
10. Olivi, P., Souza, E. C. P., Longo, E., Varela, J. A. and Bulhoes, L. O. S., Preparation and characterization of a dip-coated tin dioxide film for transparent electrodes for transmissive electrochromic devices. *J. Electrochem. Soc*., 1993, **140**, L81–L82.
11. Joss H. D., Thesis of the University of Washington, Seattle, WA, 1975.
12. Leite, E. R., Cerri, J. A., Longo, E., Varela, J. A. and Paskocima, C. A., Sintering of ultrafine undoped SnO_2 powder. *J. Eur. Ceram. Soc*., 2001, **21**, 669–675.
13. Lalande, J., Ollitrault-Fichet, R. and Boch, P., Sintering behavior of CuO-doped SnO_2. *J. Eur. Ceram. Soc*., 2000, **20**, 2415–2420.
14. Varela, J. A., Longo, E., Barelli, N., Tanaka, A. S. and Mariano, W. A., Sintering of tin oxide in different atmospheres. *Ceramica*, 1985, **31**, 241–246.
15. Cerri, J. A., Leite, E. R., Gouvêa, D. and Longo, E., Effect of cobalt(II) oxide and manganese(IV) oxide on sintering of tin(IV) oxide. *J. Am. Ceram. Soc*., 1996, **79**, 799–804.
16. Varela, J. A., Cerri, J. A., Leite, E. R., Longo, E. and Shamsuzzoha, M., Microstructural evolution during sintering of CoO doped SnO_2 ceramics. *Ceramics International*, 1999, **25**, 253–256.
17. Gaillard-Allemand, B., Pador, R., Rapin, C., Vilasi, M., Maître, A. and Steinmetz, S., Experimental study of the SnO_2–ZrO_2 phase diagram. *J. Eur. Ceram. Soc*., 2002, **22**, 2797–2803.
18. Hoenig, C. L. and Searcy, A. W., Knudsen and Langmuir evaporation studies of stannic oxide. *J. Am. Ceram. Soc*., 1966, **49**, 128–134.
19. Lange, F. F., Approach to reliable powder processing. In *Ceramic Transactions*, ed. G. L. Messing, E. R. Fuller Jr. and H. Hausner. American Ceramic Society, Westerville, OH, USA, 1989, pp. 1069–1083.
20. Maître, A. and Lefort, P., Sintering diffusional model applied to solid-solid reactions. *J. High Temp. Material Processes*, 2002, **6**, 267–282.
21. Cournil, M. and Thomas, G., Effect of the method of preparation of a mixture of powders on a solid-solid reaction. *J. Thermal Anal*., 1980, **17**, 433–435.
22. Kim, B. C., Jung, J. I., Lee, J. H. and Kim, J. J., Precipitate concentration of Co_2SnO_4 in CoO-doped SnO_2 ceramic at different oxygen chemical potentials. *Solid State Ionics*, 2001, **144**, 321–327.
23. Shannon, R. D., Revised effective ionic radii and systematic studies of interatomic distances in halides and chalcogenides. *Acta Cryst*., 1976, **A32**, 751–767.